
Revisiting Implicit Models: Sparsity Trade-offs Capability in Weight-tied Model for Vision Tasks

Haobo Song
EPFL, Switzerland
haobo.song@epfl.ch

Soumajit Majumder
Huawei
soumajit.majumder@huawei.com

Tao Lin*
Westlake University, P.R. China
lintao@westlake.edu.cn

Abstract

Implicit models such as Deep Equilibrium Models (DEQs) have garnered significant attention in the community for their ability to train infinite layer models with elegant solution-finding procedures and constant memory footprint. However, despite several attempts, these methods are heavily constrained by model inefficiency and optimization instability. Furthermore, fair benchmarking across relevant methods for vision tasks is missing. In this work, we revisit the line of implicit models and trace them back to the original weight-tied models. Surprisingly, we observe that weight-tied models are more effective, stable, as well as efficient on vision tasks, compared to the DEQ variants. Through the lens of these simple-yet-clean weight-tied models, we further study the fundamental limits in the model capacity of such models and propose the use of distinct sparse masks to improve the model capacity. Finally, for practitioners, we offer design guidelines regarding the depth, width, and sparsity selection for weight-tied models, and demonstrate the generalizability of our insights to other learning paradigms.

1 Introduction

In recent years, implicit models have gained significant attention in the field of machine learning. Different from classical deep-learning models which rely on explicit computation graphs [22], implicit models characterize their internal mechanism by some pre-specified dynamics. Classic examples of such implicit models include weight-tied models [36, 14, 43], Neural ODEs [10], and equilibrium models [4, 5]. These models begin with defining the dynamics of layer iteration and then leverage either black-box ODE solvers [10] or root-finding algorithms [4, 5] to solve the specified dynamics.

Deep Equilibrium Models or DEQs [4, 5] is a prominent implicit model in the research community. The central theme behind DEQ lies in the equilibrium state converged on an infinite-depth network, represented by a fixed point equation. This insight inspires the elegant optimization strategies of DEQ, which empowers the feasibility of achieving a constant memory footprint. Initially introduced for sequence modeling [4], DEQs were subsequently extended to computer vision applications [5].

However, achieving stable convergence to a solution in implicit-depth models necessitates substantial tuning [51], due to the model’s sensitivity to initialization and regularization [31, 6, 18, 1]. To date, an extensive line of research, e.g. [6, 18, 1], tries to improve upon these known issues of model efficiency or optimization difficulty for sequence models. Despite these attempts, these issues continue to severely bottleneck the exploration of the potential of such implicit models.

*Corresponding author

Meanwhile, the standard weight-tied models, which inspired DEQ models, and offer both computation & storage efficiency, remain largely unexamined for vision tasks across [4–6, 18, 39]. As our first contribution, we demonstrate that under the same training budget, *weight-tied models offer remarkable prediction and performance efficiency over existing DEQ variants on vision tasks.*

Leveraging the original weight-tied model as a simple proxy on the perspective of feature representation, we identify a fundamental issue, namely restricted model capability (or model expressive power), in most of the implicit models including both weight-tied models and DEQ-like models. As a remedy, and as our next contribution, we propose *multi-mask weight-tied* to implicitly induce more model capability through diverse sparsity patterns for the tied layers, while enjoying a significantly reduced computational overhead. Intuitively, storage-free, static, and non-trainable boolean masks are temporally applied to tied layers recursively, resulting in the dissimilar layer structure and thus an increased model capability. The effectiveness of such a design choice is verified by extensive results.

We summarize our contributions below:

- We demonstrate the incredible effectiveness and efficiency of standard weight-tied models over similar implicit models, such as DEQ and its variants. We emphasize heavily that the contribution of this study does not lie in the novelty of the weight-tied model itself; as such a classical idea has occurred in the community with various forms (see [section 2](#)). Rather, the contribution lies precisely in emphasizing the superior efficiency and effectiveness of such a simple baseline, which should not be omitted for evaluation when proposing advanced implicit model variants.
- We leverage the multi-mask weight-tied layer to implicitly induce model capability through the lens of a simple yet clean weight-tied model. The insights therein could further benefit the design of other implicit models in the field, which we leave for future work.
- We examine the trade-off between depth, width, and sparsity of the weight-tied layer, through extensive numerical investigations for ResNet- and Vision-Transformer-like models on CIFAR and ImageNet. We provide a clear guideline, as a novel first step, to facilitate the practitioners.
- We showcase the generalizability of our multi-mask weight-tied idea to other learning paradigms, e.g., hardware with 2:4 sparsity [12, 40], LoRA-like [24] parameter-efficient transfer learning.

2 Related Work

We provide a compact summary here due to space issues. A complete discussion is in [Appendix A](#).

Implicit models and DEQ variants. As a way of replacing explicit layers with one implicit layer and prescribed internal dynamics, implicit models have attracted wide attention from the community in recent years [2, 10, 38, 48, 4–6, 18, 1]. DEQs, as introduced in [4], is one representative approach in implicit models that finds the equilibrium of a system to eventually reach a fixed point equation. Despite the recent efforts on improving DEQ-like implicit models [6, 1, 18, 5], most studies largely ignore the original weight-tied model, despite being simple, effective, and memory inefficient, making the generalizability and practicality of DEQ variants on various use cases to be questioned; our contribution therein.

Weight-tied model. Weight-tied models, also known as weight-sharing or weight-tying models, are a type of parameter-efficient neural network architecture, in which the same set of weights is used across different layers or parts of the input [14, 13, 52, 28, 29, 43]. This architecture, as the backbone of most implicit models, has been widely studied in recent years for various tasks [50, 32, 55, 28, 43, 59, 8, 54, 29].

The existing studies for the weight-tied model focus on proposing strategies to tie different layers and do not introduce sparse masks to a shared layer like ours. As a separate line of research, weight-sharing in Neural Architecture Search (NAS) [59, 8, 54] reduces the computational overhead by sampling distinct neural architectures from a super net using sparse masks, where exponentially many architectures share weights in the same super-network and the costly training procedure is performed only once.

Model quantization and pruning. A line of seminal papers for model quantization [20, 11] employs the concept of hash functions or quantization to map weights to scalars or codebooks, thereby increasing the compression rate. This approach has been further extended to soft weight sharing [30, 56, 44, 57], where the remaining weights are assigned to the most probable clusters. However, this strategy differs from our approach of using sparse masks to enhance capability.

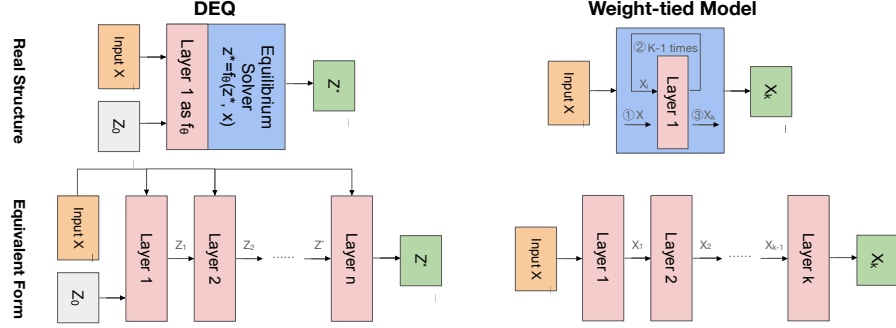


Figure 1: **DEQ and weight-tied model structure schematic diagram.** The figure above shows its real structure and the figure below shows its equivalent structure for better understanding.

Moving forward to the model pruning [46]. There exist three directions, namely i) pruning at initialization, ii) dynamic pruning during training, and iii) pruning after training. The latter two normally prune model weights relying on either importance-based or regularization-based criteria. The idea of pruning at initialization initially also relies on the magnitude-based metric [15]; however, it is then debated in several follow-up studies [42, 16, 47] that random masks—uniformly sampled and only fixes the pruning ratio per layer—are equally effective as the previous lottery ticket [15]. Note that the research of model pruning primarily aims to develop improved pruning criteria or suggest enhanced optimization strategies/objective functions for standard explicit neural networks. To the best of our knowledge, our idea of introducing various random masks to a weight-tied model is novel.

The most relevant work to our manuscript might be [7], which extends the codebook idea and learns masks on top of a fixed random weight vector to represent diverse dense layers. Specifically, masks are used to select values from a random vector (i.e., codebook) and thus form distinct dense layers. However, this approach still differs from our key idea of learning a shared weight with deterministic random binary masks, whereas our sparse masks implicitly induce model capability.

Dropout. Dropout [23] is introduced as a training technique to avoid overfitting [27, 33], by randomly modifying neural network parameters or activations [45, 3, 49, 25, 17]. Although Dropout has been extended to compress neural networks [34, 35, 19], the *stochastic* dropping idea in Dropout will only be applied to standard and explicit neural architectures, which differs from the deterministic masks of our weight-tied models.

3 Inspecting Implicit Models

3.1 Introduction to Deep Equilibrium Model

Deep Equilibrium models (DEQ) are a series of implicit models first introduced by [4]. The elegance of such approaches lies in defining the output of the network as the solution to an “infinite-depth” fixed point equation. This ingredient enables the use of some root-finding algorithms and therefore avoids the activation storage to achieve a significantly reduced memory footprint.

Formal definition of DEQ. Given a layer f parameterized by \mathbf{w} , the key hypothesis and observation of [4] rely on the convergence of the following sequence to a fixed point when increasing the depth/iteration towards infinity:

$$\lim_{i \rightarrow \infty} \mathbf{z}^{[i]} = \lim_{i \rightarrow \infty} f_{\mathbf{w}}(\mathbf{z}^{[i]}; \mathbf{x}) \equiv f_{\mathbf{w}}(\mathbf{z}^*; \mathbf{x}) = \mathbf{z}^*, \quad (1)$$

where $\mathbf{x} \in \mathbb{R}^d$ is the input injection, $\mathbf{z}^{[0]} := \mathbf{0} \in \mathbb{R}^d$, and $\mathbf{z}^{[i+1]} = f_{\mathbf{w}}(\mathbf{z}^{[i]}; \mathbf{x})$ for $i = 0, \dots, L-1$. \mathbf{z}^* represents the equilibrium point, or equivalently the root of the equation $g_{\mathbf{w}}(\mathbf{z}^t; \mathbf{x}) := f_{\mathbf{w}}(\mathbf{z}^t; \mathbf{x}) - \mathbf{z}^t = 0$, shown in the left of Figure 1. A line of attempts [4, 6, 18] improves the training/optimization phase of these infinite-layer DEQ networks through implicit differentiation and thus enjoys constant memory consumption.

3.2 Tracing Back to the Original Weight-tied Model

Despite the elegance and constant memory cost, it becomes non-trivial to probe other potentials of the implicit layers in DEQ variants, due to the suffered pitfalls of computational inefficiency as

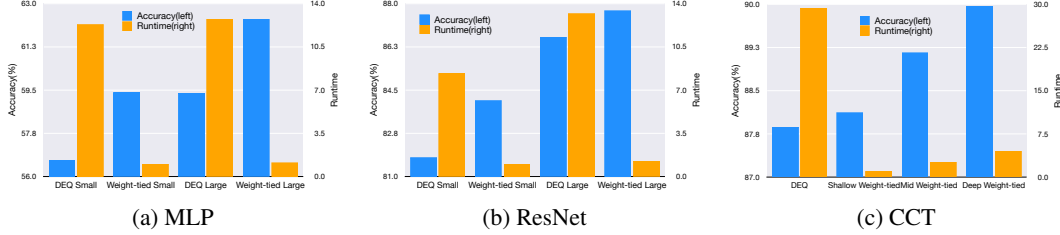


Figure 2: **Weight-tied can surpass DEQ in both computational cost and performance over different structures.** We make weight-tied and DEQ comparisons (accuracy v.s. runtime) under MLP, ResNet and CCT structures for the task of CIFAR-10 image classification (w/ data augmentation). Runtime refers to the training time used per batch. The fastest weight-tied runtime in each structure is chosen as unit time (1x), and the other model’s runtime is calculated based on unit time. All experiments are allowed sufficient training time and repeated thrice. More details are provided in Appendix. The dramatic gap in the runtime cannot be addressed by [18], which could accelerate the training by $1.7\times$.

well as the optimization instability (see results in [subsection D.1](#)). As a result, here we resort to the original weight-tied model given its simplicity and cleanness, and we believe the insights therein could be transformed into other advanced variants of implicit layers (as future work).

Formulation. The definition of the original weight-tied model largely follows the notations in [subsection 3.1](#), where a K -depth weight-tied layer (in the right of [Figure 1](#)) can be modeled explicitly by

$$\mathbf{x}_{i+1} = f_{\mathbf{w}}(\mathbf{x}_i), \quad (2)$$

where the index of i in (2) refers to the i -th weight-tied layer reusing (representing i -th tied layer). Such a design can intuitively reduce the number of parameters by a factor of K while cannot maintaining a constant memory footprint like DEQ variants².

3.3 On the Effectiveness of Weight-tied Model

Despite the simplicity and limitation of the weight-tied model, in this subsection, we thoroughly revisit this design choice and assess its efficacy by examining it with various strong competitors on three highly representative neural architectures. Such an empirical investigation is crucial to the community, given the unknown position of the weight-tied model after years of research on other advanced implicit models, as well as the surprisingly missing comparisons between the weight-tied model and DEQ variants.

Evaluation setup. For the sake of simplicity and fair comparison, we transform existing neural architectures into both weight-tied and DEQ models. Similar to the treatments in DEQ variants [4–6, 18] to guard the performance, such transformed networks (for both weight-tied and DEQ models) include a small number of not-tied layers at the bottom and top layer, while the majority of the model is constructed through the tied layer. The remaining not-tied layers in DEQ and weight-tied model are identical and constitute a very low proportion of the whole model.

We elaborate on the configuration of three considered neural architectures for weight-tied/DEQ models; other training strategies are detailed in [Appendix C](#). Note that there exists no difference between the weight-tied model and the DEQ model from the view of parameter space, though the former needs to specify the depth of the tied layer.

1. **MLP:** This MLP only contains linear layers, where the shared part comprises two weight-tied layers. We vary the model capacity, termed as *small* and *large*, by doubling the model width.
2. **ResNet:** ResNet [22] is designed similarly as the single-stream model presented in [5]. The weight-tied version has four weight-tied layers and uses similar notations of *small* and *large* as MLP.
3. **CCT:** The neural architecture of CCT (Compact Convolution Transformer [21]), considers *shallow*, *medium*, and *deep* weight-tied models, comprising of 3, 5, and 7 weight-tied modules, respectively. We transform its encoder into weight-tied and DEQ structures.

²Note that the pre-training phase of DEQ variants [4–6] almost resembles the training procedure of original weight-tied networks, and only differs in the number of training epochs.

Table 1: On the superior performance of the weight-tied model over other models.

(a) **Weight-tied model can outperform the same structured DEQ models**, e.g., original DEQ [5] and phantom gradient DEQ [18] in CIFAR-10 (with data augmentation). The weight-tied model has a depth of 8. In each test, the optimizer and learning hyperparameters for DEQ and the weight-tied model are identical and are chosen based on DEQ’s benefit. Thus, the performance of the original DEQ and phantom gradient DEQ are not comparable due to different hyperparameters.

Model Name	Accuracy	Runtime
Original Single-stream DEQ	81.75%	5.47x
Single-stream weight-tied	84.07%	1x
Original DEQ Tiny	85.76%	5.03x
Weight-tied Tiny	85.94%	1x
Original DEQ Large	91.86%	3.4x
Weight-tied Large	92.36%	1x
Phantom gradient Single-stream DEQ	85.06%	6.95x
Single-stream weight-tied	86.38%	1x
Phantom gradient DEQ Tiny	88.67%	4.90x
Weight-tied Tiny	88.59%	1x
Phantom gradient DEQ Large	94.70%	2.69x
Weight-tied Large	94.54%	1x

(b) **Weight-tied model can outperform the similar structured explicit models**. This figure shows a performance comparison between the weight-tied model and the explicit model in CIFAR-10 (with data augmentation). The notion of *small* or *large* indicates the network width. The weight-tied model has the same depth as explicit models. The explicit models are dense while the weight-tied model is sparse in order to fit similar performance as explicit models.

Model Name	Accuracy	# of Param
ResNet-20 Small	84.07%	68k
ResNet Small (weight-tied)	84.08%	35k
ResNet-20 Large	90.96%	4.3M
ResNet Large (multi-mask weight-tied)	90.99%	0.53M
CCT-7 Small	89.43%	0.96M
CCT Small (weight-tied)	89.60%	0.34M
CCT-7 Large	90.11%	3.7M
CCT Large (multi-mask weight-tied)	90.27%	0.60M

Observations. Figure 2 illustrates a thorough comparison of accuracy and runtime cost between the DEQ model and the weight-tied model for the task of CIFAR-10 classification. All CIFAR-10 experiments in this paper are equipped with standard techniques like basic normalization, random cropping, and horizontal flipping. *In all three structures examined, the weight-tied model demonstrates approximately 2% higher accuracy and a reduction in runtime ranging from 5× to 10× in both training and inference.*

Furthermore, *the advantages of the weight-tied model also hold in the multiscale cases* (an improved DEQ variant of [5]). We directly use the available open-source code of [5] and select two CIFAR models provided therein (i.e. MDEQ-Tiny, MDEQ-Large). The comparison results in Table 1a indicate that the weight-tied model can have more than 3 times runtime reduction compared to DEQ³, while maintaining a similar performance compared to the latest DEQ variant (i.e. Phantom gradient in [18]) and exhibiting a better performance compared to the original DEQ. Additionally, *Weight-tied model advantage also holds compared to explicit models*. We select ResNet-20 and CCT-7 as explicit model baselines and report our result in Table 1b.

Summary. In contrast to the existing line of work like [4–6, 18, 1] that aim to enhance the optimization quality of DEQ variants, this paper instead revisits and re-examines their fundamental building block—which is usually overlooked in their investigations—the idea of the weight-tied model. Surprisingly, as identified in Figure 2, Table 1a and Table 1b, these weight-tied models are simple yet very effective: *the weight-tied model and could outperform most of the latest DEQ variants as well as explicit models in both performance and time complexity across various neural architectures*. We believe it is worthwhile to leverage the original weight-tied model—which is clean and still an (our newly identified) very strong baseline in this field—to explore other design spaces of implicit models.

4 Multi-Mask Weight-tied Model

In this section, we explore the potential design space using the clean yet effective weight-tied model from the aspect of model capacity/model expressive power.

³It is worth noting that the hyper-parameters provided in the open-sourced GitHub repository of [5] for training these two models are not the same as the one used to retrieve the reported results in the original paper (based on their comments), thus the results may exhibit some differences.

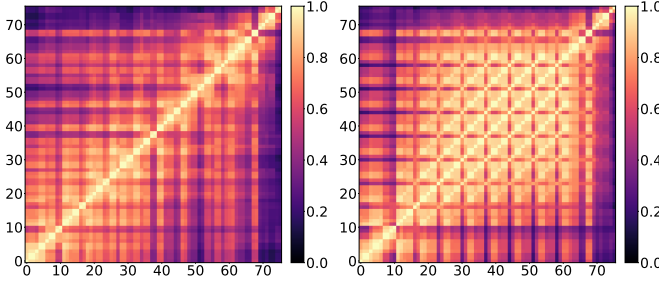


Figure 3: **The output similarity pattern** of the same-structured dense normal model (left) and weight-tied model (right), with a depth of 8 trained on the CIFAR-10 classification task. The square color in position (i, j) represents the layer output similarity of the i -th layer and j -th layer, and a higher (CKA) value implies higher similarity. The weight-tied model has more high-similarity squares.

4.1 Motivation: Limited Model Capability

Hypothesis. Despite the effectiveness of the weight-tied model, due to the coupled model weights across layers, it is natural to hypothesize that

the model capability of a weight-tied model is largely constrained.

We test this hypothesis using the tool described below. As stated in *Observation #1* (in this subsection), the feature representations extracted from each i -th tied layer of the weight-tied model exhibit a high degree of similarity, aligning with the hypothesis that *the expressive power of the tied layers are limited and cannot capture distinct feature representations as normal not-tied networks.*

Toolbox. Inspired by [37], we utilize the linear version of Centered Kernel Alignment (CKA) [26], as a robust way to measure the *layer-wise feature activation similarities* of every layer pair, and thus reliably identify architecturally corresponding layers. These layer similarities will be presented in a squared heatmap, where the similarity between the i -th and j -th layers is represented in the (i, j) and (j, i) positions of the square. We briefly outline the formulation of linear CKA below:

$$\text{CKA}(\mathbf{K}, \mathbf{L}) = \frac{\text{HSIC}(\mathbf{K}, \mathbf{L})}{\sqrt{\text{HSIC}(\mathbf{K}, \mathbf{K})\text{HSIC}(\mathbf{L}, \mathbf{L})}}, \quad (3)$$

where $\mathbf{K} := \mathbf{X}\mathbf{X}^\top$ and $\mathbf{L} := \mathbf{Y}\mathbf{Y}^\top$ represent the similarities between a pair of examples according to the representations in \mathbf{X} or \mathbf{Y} . The CKA empowers the robust quantitation by normalizing the HSIC metric, a.k.a. Hilbert-Schmidt Independence Criterion (measuring the similarity of these similarity matrices). More details can be found in [Appendix B](#) and [37].

Observation #1: a high layer-wise similarity emerged in the weight-tied model, indicating a constrained expressive power. Figure 3 depicts a layer similarity heatmap in both the normal (not-tied) model and the weight-tied model. The patterns shown in the heatmap are distinct between these two models. Specifically, the weight-tied model illustrates a notable section that displays a *high output similarity*, which can be attributed to the weight-tied module. This observation suggests that the output produced by the weight-tied module exhibits a higher degree of similarity. Given the identical parameters in the weight-tied layer, this similarity implies that the weight-tied model is in the way of converging, similar to what happened in DEQ [4].

4.2 Sparsity Trade-off Capacity for Weight-tied Model

An intuitive and straightforward idea could be of using diverse sparse masks on the tied layers to induce larger capability for the weight-tied layers, as illustrated in [Figure 4](#). We term this design as **multi-mask weight-tied** model, where these boolean masks are distinct, static, and non-trainable across the training, and can be determined before the training phase. The storage overhead of these boolean masks can be avoided by using a *random generator* to generate deterministic masks on the fly with several scalar seeds per forward and backward pass.

The recursive procedure of a K -depth multi-mask weight-tied model can be expressed as,

$$\mathbf{x}_{i+1} = f_{\mathbf{w} \odot \mathbf{m}_i}(\mathbf{x}_i), \quad (4)$$

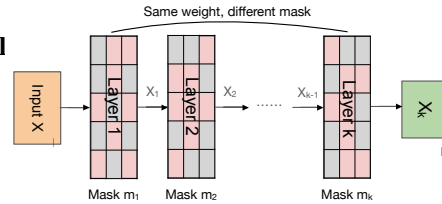
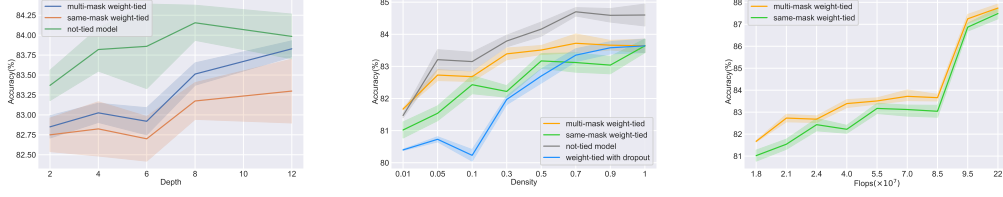


Figure 4: **An illustration of multi-mask weight-tied model.** The structure shown in the graph is in equivalent form, only one physical layer with K unique and pre-determined boolean masks exist.



(a) Varying depths with density 0.5. (b) Varying densities with depth of 8 (c) Varying FLOPs.

Figure 5: Multi-mask weight-tied models can surpass same-mask weight-tied models regarding different depths, densities, and FLOPs. All tests are conducted on the CIFAR-10 classification task, for ResNet-like models (similar to single-stream DEQ structure) with 3 independent runs. Figure (a) is evaluated among different weight-tied depths while all model density=0.5. Figure (b) is evaluated among different weight-tied densities while weight-tied depth and corresponding structure in the not-tied model is equal to 8. Dropout implemented on the weight-tied model is also added as a comparison here. Figure (c) is tested among different model widths and weight-tied densities while the weight-tied depth is fixed to 8. More details are in Appendix.

where the masking \mathbf{m}_i of i -th tied layer \mathbf{w} will only be applied during the forward and backward pass, and the parameter number will reduce with a ratio of $1 - s^k$ if masks are generated independently, where s is sparsity ratio of masks.

It is noteworthy to mention the sparsity within the tied layer would significantly trade off the model capability and thus determine the eventual model performance. We will elaborate on this point in [section 5](#) with detailed practical guidelines.

Evaluation setup. The benefits of the proposed multi-mask weight-tied method can be validated through a fair comparison between (1) the multi-mask weight-tied model, (2) the same-mask weight-tied model, and (3) the conventional model (i.e. not-tied model). Note that here we omit the comparison with DEQ, due to the superior performance of the weight-tied model over DEQ variants as examined in [subsection 3.3](#).

Following a similar experimental setup in [subsection 3.3](#), we consider the image classification task on the CIFAR-10 dataset and state some additional treatments for the multi-mask weight-tied model. For the sake of simplicity, a naive pruning approach referred to as “*equal per layer*” [16, 41] was employed to ensure that each layer maintains the same ratio of remaining nodes. The weight-tied module was the only module that was pruned while other normal modules at the bottom and top layers remain dense.

Observations: *In a variety of depths, densities, and training FLOPs, multi-mask weight-tied models can significantly outperform same-mask weight-tied, and thus justify our intuition.* The performance curves regarding various layer depths and layer densities of the weight-tied layers, as well as different numbers of training FLOPs⁴, are illustrated in [Figure 5](#) respectively. The results show that the multi-mask weight-tied models exhibit a performance benefit of approximately 0.2% to 1% in all cases. In some instances, the multi-mask weight-tied model even surpasses the not-tied model which has 8 times more parameters in the weight-tied layer. Moreover, regarding the similarity with the dropout method, we also include it in our baseline. The results also indicate that the multi-mask weight-tied model can also outperform dropout in all cases.

4.3 Interpreting Multi-mask Weight-tied Model

In previous subsections, motivated by the enormous potential of the weight-tied model in both efficiency and effectiveness, as well as the limited model expressive power constrained by the weight-tied layers, we extend the concept of masking and design a novel multi-mask weight-tied model. Despite the identified effectiveness and efficiency of the multi-mask weight-tied models, the reasons behind these empirical gains remain unclear. In this subsection, we further leverage the dynamics in the feature space (using the CKA tool stated in [section 4](#)) to unravel the underlying principles of the multi-mask weight-tied model.

⁴The sparsity injected in the tied layers would naturally bring an improved efficiency gain.

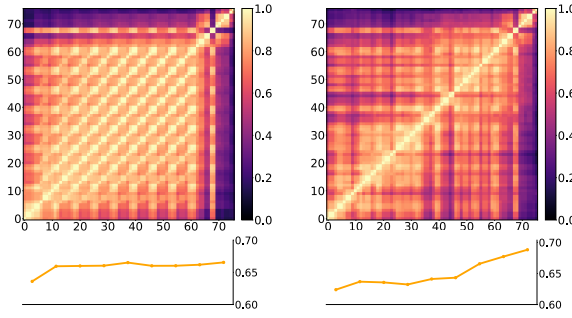
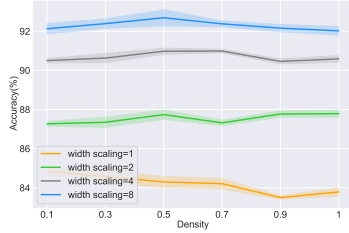
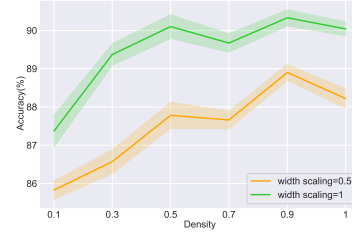


Figure 6: Multi-mask weight-tied approach can erase high output similarity pattern. The figure shows output similarity inside the same-structured same-mask weight-tied model (up left) and multi-mask weight-tied model (up-right) on the CIFAR-10 classification task, for models with a density of 0.1 and depth of 8. The square color in position (i, j) represents layer output similarity in the i -th layer and j -th layer. The bottom figure shows model performance change with layer number increasing. The performance is tested through linear probing after each tied layer.



(a) ResNet-like model.



(b) CCT-like model.

Figure 7: Sparse multi-mask weight-tied model can outperform dense weight-tied model. We evaluate model performance under different densities and model widths, with a fixed depth for the CIFAR-10 classification task (8 for the ResNet-like model and 7 for CCT-like model). Models are trained in the same number of FLOPs.

Observation #2: multi-mask weight-tied approach can erase high output similarity pattern. We can witness from [Figure 6](#) that, after applying diverse masks to the weight-tied model, the patterns observed in the output similarity squares differ significantly between the case of multi-mask weight-tied model and that of same-mask. Specifically, with the multi-mask weight-tied model, the high output similarity region of the weight-tied module disappears, while this high similarity region is accentuated in the case of the same-mask one.

The diminishing of the high output similarity region can be attributed to the diverse sparse mask associated with each tied layer of the multi-mask weight-tied model, resulting in a dissimilar layer in each reused time and thus a decrease in output similarity. Conversely, when using the same-mask weight-tied model, the sparsified layer remains the same across all weight-tied layers, leading to an increase in output similarity due to the constrained model capability. Such observation is aligned with our initial intuition of leveraging multi-mask as an implicit way to increase the model’s expressive power.

The explanation provided above is also consistent with the trend of performance observed in each tied layer illustrated at the bottom of [Figure 6](#). More precisely, we perform Linear Probing used in [26] on the trained model per tied layer, as a way to examine the quality of extracted feature representations upon each newly included tied layer. The performance of the multi-mask weight-tied model continues to improve as the more tied layer is included while that of the same-mask one remains relatively stable: for example, after 8 weight-tied layers, about 3% performance gain can be observed by the multi-mask one, as compared to the same-mask.

Observation #3: a larger depth strengthens the high output similarity pattern. We can witness from [Figure 11](#) of [Appendix D](#) that different weight-tied depths result in a varied level of output similarity in the weight-tied model. Though models with a higher depth of weight-tied layers exhibit higher similarity, it does not necessarily translate to improved performance, given the degraded performance for depth = 20. This is likely because the weight-tied layers are close to converging in the early layers and the later layers are unable to make any further contributions to performance, while only increasing the computational costs.

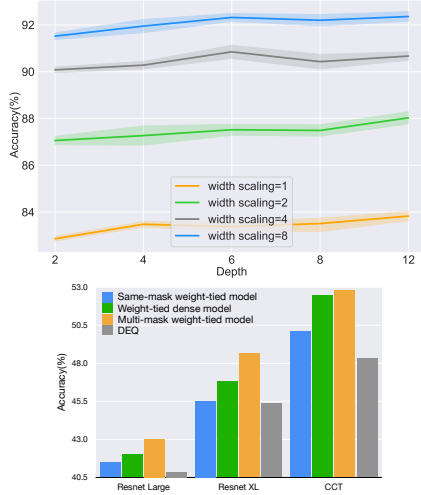


Figure 8: **Model width is more essential to performance than weight-tied depth.** All tests are conducted in ResNet-like models on the CIFAR-10 classification task. We evaluate model performance under different model widths and weight-tied depths while the weight-tied density is fixed at 0.5. Model width is controlled by multiplying every layer with a width scaling factor.

Mask density	CIFAR-10 Acc (%)	ImageNet32 Acc (%)
0.3	90.63	42.97
0.5	90.98	43.05
0.7	90.99	42.94
0.9	90.46	42.66
1	90.59	42.04

(a) Multi-mask weight-tied model surpasses the dense weight-tied model, same-mask weight-tied model, and DEQ, for ResNet- and CCT-like architecture on ImageNet32. Weight-tied models use a density of 0.5.

(b) Multi-mask weight-tied model surpasses the dense weight-tied model, for ResNet-Large models under different densities with a fixed depth of 8.

Figure 9: **Sparse multi-mask weight-tied model can outperform other variants on ImageNet32.** ImageNet32 is a down-sampled ImageNet dataset including all ImageNet images. ResNet-XL is two times wider than ResNet-Large. All models are trained in the same number of FLOPs.

5 Trade-offs and Practical Guidelines

Despite the empirical effectiveness of the multi-mask weight-tied model, it may be non-trivial to identify a proper configuration in practice. When transforming a conventional neural architecture to a multi-mask weight-tied model, there exist at least three hyperparameters to configure, namely the depth, mask density, and model width, of the multi-mask weight-tied part. A different combination of these parameters can result in noticeable variations and trade-offs in model performance. Therefore, in this section, we provide some crucial insights to study the trade-off of these parameters and provide a guideline for practitioners.

5.1 Don’t Increase Model Depth, Increase Model Width

Rather than the depth of weight-tied layers, model width is more essential to the model performance. Figure 8 illustrates the performance under various weight-tied depths and model widths (we fix model density to 0.5 to avoid the influence of mask density). We can witness that *the benefits brought by increasing the depth in the weight-tied layers are far behind that of increasing the model width*, where a 12-depth multi-mask weight-tied model significantly lags behind a 2-depth multi-mask weight-tied which is 2 times wider. Furthermore, a large value of depth in the weight-tied layer may not always correspond to the improved performance: it intuitively explains DEQ’s difficulty in (significantly) surpassing the simple weight-tied model in Figure 2, in which an infinite depth may not guarantee better performance than finite depth.

Practical guide #1: The model width matters, rather than the depth of weight-tied layers: practically it is sufficient to use a depth of 6 or 8 in the weight-tied layers to ensure reasonably good performance.

5.2 On the Superior Empirical Effectiveness of Multi-mask Weight-tied Model

Given the practical guide #1 found in subsection 5.1, in this section, we consider experiments for the multi-mask weight model with a fixed weight-tied depth while varying the mask densities and model widths.

Table 2: **Multi-mask remains superior performance with 2:4 fine-grained structured sparsity** on CIFAR-10 classification task. The “Small” and “Large” refer to different model widths. Results are averaged over three trials.

Model Size	ResNet-like model		CCT-like model	
	2:4 sparsity	unstructured sparsity	2:4 sparsity	unstructured sparsity
Small	83.16 \pm 0.10%	83.51 \pm 0.14%	88.08 \pm 0.63%	87.78 \pm 0.34%
Large	90.44 \pm 0.21%	90.43 \pm 0.31%	89.56 \pm 0.46%	90.10 \pm 0.31%

Sparse multi-mask weight-tied model can outperform dense weight-tied model. In addition to the effectiveness of the multi-mask weight-tied model identified in Figure 5, the results in Figure 7a move one step further by comparing the sparse multi-mask weight-tied model with the dense counterparts. The superior effectiveness of the multi-mask weight-tied model can be justified by the fact that: *when trained with the same number of FLOPs, the multi-mask weight-tied model can outperform the dense weight-tied model in each model width* (similar pattern persists when training models with the same amount of training epochs). Such an observation is also consistent across different neural architectures, as verified by a Vision-Transformer model in Figure 7b.

On the hardware-friendly multi-mask weight-tied model. The 2:4 fine-grained structured sparse network [12, 58] trades off the benefits of both unstructured fine-grained sparsity and structured coarse-grained sparsity, by accelerating matrix multiplication at least two times through NVIDIA’s sparse tensor cores [40]. As the 2:4 fine-grained structured sparsity inherently exhibits 50% sparsity, which aligns with our suggested sparsity ratio for the multi-mask weight-tied model, Table 2 demonstrates that *our multi-mask weight-tied model unleash the potential of delivering performance gains across sparsity structures, while maintaining high levels of computation efficiency and learning effectiveness.*

Practical guide #2: Instead of using a dense weight-tied model, the multi-mask weight-tied model is a more appealing choice. A density of 0.5 usually achieves an optimal performance across all densities for ResNet-like architectures, while a density of 0.9 might be more suitable for Transformer-like architectures.

5.3 Examining the Generalizability of the Findings on ImageNet

In this subsection, we examine the effectiveness and generalizability of the two key findings for the multi-mask weight-tied model, on the challenging ImageNet⁵ dataset for both ResNet-like and Transformer-like neural architectures. In Figure 9a, the multi-mask weight-tied model again outperforms both the dense weight-tied model and the sparse weight-tied model with the same mask across layers. In Figure 9b, the sparse multi-mask weight-tied model can still outperform the dense weight-tied model in ImageNet32 and reach the best performance at the density of 0.5.

5.4 Case Study: Extending to LoRA for Parameter-efficient Transfer Learning

The idea of the multi-mask weight-tied model has great potential to empower other learning paradigms, as showcased below.

Multi-mask weight-tied LoRA. Transfer Learning from pre-trained foundation models [9] is now the prevalent paradigm. LoRA [24], as one of the parameter-efficient transfer learning techniques for downstream tasks, proposes to model the incremental update of the pre-trained weights $\mathbf{W} \in \mathbb{R}^{d_1 \times d_2}$ through low-rank approximations $\mathbf{W} = \mathbf{W}_{\text{pre-trained}} + \Delta$, where $\Delta := \mathbf{B}\mathbf{A}$ is trainable, $\mathbf{A} \in \mathbb{R}^{r \times d_2}$, $\mathbf{B} \in \mathbb{R}^{d_1 \times r}$, and $r \ll \{d_1, d_2\}$. Extending the multi-mask weight-tied to LoRA is equivalent to considering $\mathbf{W} = \mathbf{W}_{\text{pre-trained}} + \sum_{i=1}^d (\mathbf{m}_{i,1} \odot \mathbf{B})(\mathbf{m}_{i,2} \odot \mathbf{A})$, where d indicates the depth of the multi-mask weight-tied model and $\mathbf{m}_{\cdot, \cdot}$ corresponds to the choice of deterministic binary mask per layer.

The multi-mask weight-tied idea enables greatly improving the model capability of LoRA while preserving the storage and computation efficiency, resulting in 1% higher overall performance in VTAB-1k task, as 2-depth and 4-depth multi-mask LoRA evidenced in Table 3.

⁵Due to the computational feasibility, we only afford to evaluate on a down-sampled ImageNet. However, we believe the success therein can be transferred to the original ImageNet as well as other large-scale datasets.

Table 3: **Multi-mask LoRA for parameter-efficient transfer learning.** Multi-mask LoRA achieves better overall performance, *1% higher than LoRA*, while the parameter numbers remain the same. We follow the experimental settings in [60] and report multi-mask LoRA results in the VTAB-1k benchmark. The base model used is ViT-B/16 pre-trained on ImageNet-22K, and LoRA/multi-mask LoRA contain 0.29M trainable parameters. Both LoRA and multi-mask LoRA have rank of 8 and are trained for 100 epochs. Results are averaged over three trials.

Model Name	Natural					Specialized		Structured					Average
	CIFAR-100	DTD	Flower102	Pets	SVHN	Eurosat	Resisc45	Clevr-Count	Clevr-Dist	DMLab	dSpr-Ori	sNORB-Azim	
LoRA	67.10 $\pm 0.31\%$	69.89 $\pm 0.52\%$	98.95 $\pm 0.05\%$	90.58 $\pm 0.27\%$	84.20 $\pm 0.70\%$	95.34 $\pm 0.24\%$	85.93 $\pm 0.13\%$	82.68 $\pm 0.20\%$	67.92 $\pm 0.52\%$	49.68 $\pm 0.15\%$	45.54 $\pm 0.20\%$	30.80 $\pm 0.30\%$	72.38%
multi-mask LoRA (d=2)	69.28 $\pm 0.53\%$	71.45 $\pm 0.26\%$	99.06 $\pm 0.09\%$	91.21 $\pm 0.31\%$	85.01 $\pm 1.08\%$	95.55 $\pm 0.21\%$	86.48 $\pm 0.11\%$	82.80 $\pm 0.17\%$	69.05 $\pm 0.41\%$	50.58 $\pm 0.75\%$	46.04 $\pm 0.05\%$	31.94 $\pm 0.20\%$	73.20%
multi-mask LoRA (d=4)	69.01 $\pm 0.08\%$	72.18 $\pm 0.62\%$	99.06 $\pm 0.03\%$	91.20 $\pm 0.17\%$	87.07 $\pm 0.60\%$	95.76 $\pm 0.09\%$	85.96 $\pm 0.15\%$	82.77 $\pm 0.34\%$	69.11 $\pm 0.34\%$	50.90 $\pm 0.88\%$	45.84 $\pm 0.20\%$	32.09 $\pm 0.31\%$	73.41%

6 Discussion and Conclusion

In this paper, we first identify that DEQ is subjected to model inefficiency and optimization instability. To address these limitations, we revisit implicit models and trace them back to the original weight-tied models. Our experiments indicate that weight-tied models can outperform existing DEQs in terms of both performance and computational expense. To further enhance the model capacity of weight-tied models, we propose the use of multi-mask weight-tied models. The superior performance and effectiveness of multi-mask weight-tied models, in comparison to same-mask weight-tied models, dense weight-tied models, and DEQs, are established by empirical experiments across various model structures and tasks. To facilitate the practical use of multi-mask weight-tied models, we examine the trade-off between depth, width, and sparsity of the weight-tied layer and indicate that relatively wider and sparser models are preferred.

References

- [1] A. Agarwala and S. S. Schoenholz. Deep equilibrium networks are sensitive to initialization statistics. In *International Conference on Machine Learning*, pages 136–160. PMLR, 2022.
- [2] B. Amos and J. Z. Kolter. Optnet: Differentiable optimization as a layer in neural networks. In *International Conference on Machine Learning*, pages 136–145. PMLR, 2017.
- [3] J. Ba and B. Frey. Adaptive dropout for training deep neural networks. *Advances in neural information processing systems*, 26, 2013.
- [4] S. Bai, J. Z. Kolter, and V. Koltun. Deep equilibrium models. *Advances in Neural Information Processing Systems*, 32, 2019.
- [5] S. Bai, V. Koltun, and J. Z. Kolter. Multiscale deep equilibrium models. *Advances in Neural Information Processing Systems*, 33:5238–5250, 2020.
- [6] S. Bai, V. Koltun, and J. Z. Kolter. Stabilizing equilibrium models by jacobian regularization. *arXiv preprint arXiv:2106.14342*, 2021.
- [7] Y. Bai, H. Wang, X. Ma, Y. Zhang, Z. Tao, and Y. Fu. Parameter-efficient masking networks. *Advances in Neural Information Processing Systems*, 2022.
- [8] G. Bender, H. Liu, B. Chen, G. Chu, S. Cheng, P.-J. Kindermans, and Q. V. Le. Can weight sharing outperform random architecture search? an investigation with tunas. In *2020 IEEE/CVF Conference on Computer Vision and Pattern Recognition (CVPR)*, pages 14311–14320. IEEE, 2020.
- [9] R. Bommasani, D. A. Hudson, E. Adeli, R. Altman, S. Arora, S. von Arx, M. S. Bernstein, J. Bohg, A. Bosselut, E. Brunskill, et al. On the opportunities and risks of foundation models. *arXiv preprint arXiv:2108.07258*, 2021.
- [10] R. T. Chen, Y. Rubanova, J. Bettencourt, and D. K. Duvenaud. Neural ordinary differential equations. In *Advances in neural information processing systems*, volume 31, 2018.
- [11] W. Chen, J. Wilson, S. Tyree, K. Weinberger, and Y. Chen. Compressing neural networks with the hashing trick. In *International conference on machine learning*, pages 2285–2294. PMLR, 2015.
- [12] J. Choquette, W. Gandhi, O. Giroux, N. Stam, and R. Krashinsky. Nvidia a100 tensor core gpu: Performance and innovation. *IEEE Micro*, 41(2):29–35, 2021.
- [13] R. Dabre and A. Fujita. Recurrent stacking of layers for compact neural machine translation models. In *Proceedings of the AAAI Conference on Artificial Intelligence*, volume 33, pages 6292–6299, 2019.
- [14] M. Dehghani, S. Gouws, O. Vinyals, J. Uszkoreit, and L. Kaiser. Universal transformers. In *International Conference on Learning Representations*, 2019.
- [15] J. Frankle and M. Carbin. The lottery ticket hypothesis: Finding sparse, trainable neural networks. In *International Conference on Learning Representations*, 2019.
- [16] J. Frankle, G. K. Dziugaite, D. Roy, and M. Carbin. Pruning neural networks at initialization: Why are we missing the mark? In *International Conference on Learning Representations*, 2021.
- [17] Y. Gal and Z. Ghahramani. Dropout as a bayesian approximation: Representing model uncertainty in deep learning. In *international conference on machine learning*, pages 1050–1059. PMLR, 2016.
- [18] Z. Geng, X.-Y. Zhang, S. Bai, Y. Wang, and Z. Lin. On training implicit models. *Advances in Neural Information Processing Systems*, 34:24247–24260, 2021.
- [19] A. N. Gomez, I. Zhang, S. R. Kamalakara, D. Madaan, K. Swersky, Y. Gal, and G. E. Hinton. Learning sparse networks using targeted dropout. *arXiv preprint arXiv:1905.13678*, 2019.

- [20] S. Han, H. Mao, and W. J. Dally. Deep compression: Compressing deep neural networks with pruning, trained quantization and huffman coding. *arXiv preprint arXiv:1510.00149*, 2015.
- [21] A. Hassani, S. Walton, N. Shah, A. Abuduweili, J. Li, and H. Shi. Escaping the big data paradigm with compact transformers. *arXiv preprint arXiv:2104.05704*, 2021.
- [22] K. He, X. Zhang, S. Ren, and J. Sun. Deep residual learning for image recognition. In *Proceedings of the IEEE conference on computer vision and pattern recognition*, pages 770–778, 2016.
- [23] G. E. Hinton, N. Srivastava, A. Krizhevsky, I. Sutskever, and R. R. Salakhutdinov. Improving neural networks by preventing co-adaptation of feature detectors. *arXiv preprint arXiv:1207.0580*, 2012.
- [24] E. J. Hu, yelong shen, P. Wallis, Z. Allen-Zhu, Y. Li, S. Wang, L. Wang, and W. Chen. LoRA: Low-rank adaptation of large language models. In *International Conference on Learning Representations*, 2022.
- [25] D. P. Kingma, T. Salimans, and M. Welling. Variational dropout and the local reparameterization trick. *Advances in neural information processing systems*, 28, 2015.
- [26] S. Kornblith, M. Norouzi, H. Lee, and G. Hinton. Similarity of neural network representations revisited. In *International Conference on Machine Learning*, pages 3519–3529. PMLR, 2019.
- [27] A. Labach, H. Salehinejad, and S. Valaee. Survey of dropout methods for deep neural networks. *arXiv preprint arXiv:1904.13310*, 2019.
- [28] Z. Lan, M. Chen, S. Goodman, K. Gimpel, P. Sharma, and R. Soricut. Albert: A lite bert for self-supervised learning of language representations. In *International Conference on Learning Representations*, 2020.
- [29] G. Li, M. Müller, B. Ghanem, and V. Koltun. Training graph neural networks with 1000 layers. In *International conference on machine learning*, pages 6437–6449. PMLR, 2021.
- [30] Y. Li, S. Gu, C. Mayer, L. V. Gool, and R. Timofte. Group sparsity: The hinge between filter pruning and decomposition for network compression. In *Proceedings of the IEEE/CVF conference on computer vision and pattern recognition*, pages 8018–8027, 2020.
- [31] D. Linsley, A. Karkada Ashok, L. N. Govindarajan, R. Liu, and T. Serre. Stable and expressive recurrent vision models. *Advances in Neural Information Processing Systems*, 33:10456–10467, 2020.
- [32] K. Liu, R. Ding, Z. Zou, L. Wang, and W. Tang. A comprehensive study of weight sharing in graph networks for 3d human pose estimation. In *European Conference on Computer Vision*, pages 318–334. Springer, 2020.
- [33] Z. Liu, Z. Xu, J. Jin, Z. Shen, and T. Darrell. Dropout reduces underfitting. *arXiv preprint arXiv:2303.01500*, 2023.
- [34] D. Molchanov, A. Ashukha, and D. Vetrov. Variational dropout sparsifies deep neural networks. In *International Conference on Machine Learning*, pages 2498–2507. PMLR, 2017.
- [35] K. Neklyudov, D. Molchanov, A. Ashukha, and D. P. Vetrov. Structured bayesian pruning via log-normal multiplicative noise. *Advances in Neural Information Processing Systems*, 30, 2017.
- [36] J. Ngiam, Z. Chen, D. Chia, P. Koh, Q. Le, and A. Ng. Tiled convolutional neural networks. *Advances in neural information processing systems*, 23, 2010.
- [37] T. Nguyen, M. Raghu, and S. Kornblith. Do wide and deep networks learn the same things? uncovering how neural network representations vary with width and depth. *arXiv preprint arXiv:2010.15327*, 2020.
- [38] V. Niculae, A. Martins, M. Blondel, and C. Cardie. Sparsemap: Differentiable sparse structured inference. In *International Conference on Machine Learning*, pages 3799–3808. PMLR, 2018.

- [39] A. Pokle, Z. Geng, and Z. Kolter. Deep equilibrium approaches to diffusion models. In *Advances in neural information processing systems*, 2022.
- [40] J. Pool, A. Sawarkar, and J. Rodge. Accelerating inference with sparsity using the nvidia ampere architecture and nvidia tensorrt. *NVIDIA Developer Technical Blog*, <https://developer.nvidia.com/blog/accelerating-inference-with-sparsity-using-ampere-and-tensorrt>, 2021.
- [41] I. Price and J. Tanner. Dense for the price of sparse: Improved performance of sparsely initialized networks via a subspace offset. In *International Conference on Machine Learning*, pages 8620–8629. PMLR, 2021.
- [42] J. Su, Y. Chen, T. Cai, T. Wu, R. Gao, L. Wang, and J. D. Lee. Sanity-checking pruning methods: Random tickets can win the jackpot. *Advances in Neural Information Processing Systems*, 33:20390–20401, 2020.
- [43] S. Takase and S. Kiyono. Lessons on parameter sharing across layers in transformers. *arXiv preprint arXiv:2104.06022*, 2021.
- [44] K. Ullrich, E. Meeds, and M. Welling. Soft weight-sharing for neural network compression. In *International Conference on Learning Representations*, 2017.
- [45] L. Wan, M. Zeiler, S. Zhang, Y. Le Cun, and R. Fergus. Regularization of neural networks using dropconnect. In *International conference on machine learning*, pages 1058–1066. PMLR, 2013.
- [46] H. Wang, C. Qin, Y. Bai, and Y. Fu. Why is the state of neural network pruning so confusing? on the fairness, comparison setup, and trainability in network pruning. *arXiv preprint arXiv:2301.05219*, 2023.
- [47] H. Wang, C. Qin, Y. Bai, Y. Zhang, and Y. Fu. Recent advances on neural network pruning at initialization. In *Proceedings of the International Joint Conference on Artificial Intelligence, IJCAI, Vienna, Austria*, pages 23–29, 2022.
- [48] P.-W. Wang, P. Donti, B. Wilder, and Z. Kolter. Satnet: Bridging deep learning and logical reasoning using a differentiable satisfiability solver. In *International Conference on Machine Learning*, pages 6545–6554. PMLR, 2019.
- [49] S. Wang and C. Manning. Fast dropout training. In *international conference on machine learning*, pages 118–126. PMLR, 2013.
- [50] X. Wang, A. Bao, Y. Cheng, and Q. Yu. Weight-sharing multi-stage multi-scale ensemble convolutional neural network. *International Journal of Machine Learning and Cybernetics*, 10(7):1631–1642, 2019.
- [51] E. Winston and J. Z. Kolter. Monotone operator equilibrium networks. *Advances in Neural Information Processing Systems*, 33:10718–10728, 2020.
- [52] Y. Xia, T. He, X. Tan, F. Tian, D. He, and T. Qin. Tied transformers: Neural machine translation with shared encoder and decoder. In *Proceedings of the AAAI conference on artificial intelligence*, volume 33, pages 5466–5473, 2019.
- [53] T. Xiao, Y. Li, J. Zhu, Z. Yu, and T. Liu. Sharing attention weights for fast transformer. *arXiv preprint arXiv:1906.11024*, 2019.
- [54] L. Xie, X. Chen, K. Bi, L. Wei, Y. Xu, L. Wang, Z. Chen, A. Xiao, J. Chang, X. Zhang, et al. Weight-sharing neural architecture search: A battle to shrink the optimization gap. *ACM Computing Surveys (CSUR)*, 54(9):1–37, 2021.
- [55] Z. Yang, W. Chen, F. Wang, and B. Xu. Unsupervised neural machine translation with weight sharing. In *Proceedings of the 56th Annual Meeting of the Association for Computational Linguistics (Volume 1: Long Papers)*, pages 46–55, 2018.
- [56] S. Ye, T. Zhang, K. Zhang, J. Li, J. Xie, Y. Liang, S. Liu, X. Lin, and Y. Wang. A unified framework of dnn weight pruning and weight clustering/quantization using admm. *arXiv preprint arXiv:1811.01907*, 2018.

- [57] D. Zhang, H. Wang, M. Figueiredo, and L. Balzano. Learning to share: Simultaneous parameter tying and sparsification in deep learning. In *International Conference on Learning Representations*, 2018.
- [58] Y. Zhang, M. Lin, Z. Lin, Y. Luo, K. Li, F. Chao, Y. WU, and R. Ji. Learning best combination for efficient n:m sparsity. In A. H. Oh, A. Agarwal, D. Belgrave, and K. Cho, editors, *Advances in Neural Information Processing Systems*, 2022.
- [59] Y. Zhang, Z. Lin, J. Jiang, Q. Zhang, Y. Wang, H. Xue, C. Zhang, and Y. Yang. Deeper insights into weight sharing in neural architecture search. *arXiv preprint arXiv:2001.01431*, 2020.
- [60] Y. Zhang, K. Zhou, and Z. Liu. Neural prompt search. *arXiv preprint arXiv:2206.04673*, 2022.

A Related Work

Implicit models and DEQ variants. As a way of replacing explicit layers with one implicit layer and prescribed internal dynamics, implicit models have attracted wide attention from the community in recent years [2, 10, 38, 48, 4–6, 18, 1]. The DEQ model, as introduced by [4], is one representative approach in implicit models that finds the equilibrium of a system to eventually reach a fixed point equation. Rather than considering the orthogonal, computationally expensive, or numerical unstable Neural ODE [10], in this work, we take the more scalable and promising line of the deep equilibrium approach as stated in the literature [5, 18, 39], to examine the latest progress in implicit models.

DEQ, in its original form [4], severely suffers from the issues like training instability and computational inefficiency. The perspective of training instability was later discussed in [6] by proposing a regularization scheme for the ill-conditioned Jacobian to stabilize the learning. The work of [1] theoretically discusses this instability from the view of initialization statistics, though only toy examples are provided on MNIST with no significant gains being observed when compared to the best-performing networks. The work of [18] instead pursues to approximate the exact calculation of the Jacobian-inverse term and thus accelerates the training by at most $1.7 \times$ while still achieving performance on par with that of DEQ variants. Regarding deep learning applications, the work of [5] propose *Multiscale DEQ* (MDEQ) to improve upon image classification, while [39] take all recent ingredients of DEQ variants and adapt DEQ to diffusion models.

However, it is noteworthy to mention that these recent researches largely ignore the original weight-tied model, despite being simple, effective, and memory inefficient, making the generalizability and practicality of DEQ variants on various use cases to be questioned; our contribution therein.

Weight-tied model. Weight-tied models, also known as weight-sharing or weight-tying models, are a type of parameter-efficient neural network architecture, in which the same set of weights is used across different layers or parts of the input [14, 13, 52, 28, 29, 43]. This architecture, as the backbone of most implicit models, has been widely studied in recent years for various tasks [50, 32, 55, 28, 43, 59, 8, 54, 29]. For instance, the Universal Transformer proposed in [14] ties the parameters through one Transformer layer; such an idea was later employed in [13, 28]. In addition, the work of [52] introduce an encoder-decoder architecture that shares parameters between the encoder and decoder parts. The work of [53] propose a method to share attention weights to speed up the computation of Transformers. The work of [43] take this idea further and proposes three strategies to tie the parameters of different layers (with various combinations), instead of just sharing the parameters of one layer with all layers.

The aforementioned studies focus on proposing strategies to tie different layers and do not introduce sparse masks to a shared layer like ours. As a separate line of research, weight-sharing in Neural Architecture Search (NAS) [59, 8, 54] reduces the computational overhead by sampling distinct neural architectures from a super net using sparse masks, where exponentially many architectures share weights in the same super-network and the costly training procedure is performed only once.

Model quantization and pruning. A line of seminal papers for model quantitation [20, 11] employs the concept of hash functions or quantization to map weights to scalars or codebooks, thereby increasing the compression rate. This approach has been further extended to soft weight sharing [30, 56, 44, 57], where the remaining weights are assigned to the most probable clusters. However, this strategy differs from our approach of using sparse masks to enhance capability.

Moving forward to the model pruning [46]. There exist three directions, namely i) pruning at initialization, ii) dynamic pruning during training, and iii) pruning after training. The latter two normally prune model weights relying on either importance-based or regularization-based criteria. The idea of pruning at initialization initially also relies on the magnitude-based metric [15]; however, it is then debated in several follow-up studies [42, 16, 47] that random masks—uniformly sampled and only fixes the pruning ratio per layer—are equally effective as the previous lottery ticket [15]. Note that the research of model pruning primarily aims to develop improved pruning criteria or suggest enhanced optimization strategies/objective functions for standard explicit neural networks. To the best of our knowledge, our idea of introducing various random masks to a weight-tied model is novel.

The most relevant work to our manuscript might be [7], which extends the codebook idea and learns masks on top of a fixed random weight vector to represent diverse dense layers. Specifically, masks are used to select values from a random vector (i.e., codebook) and thus form distinct dense layers.

However, this approach still differs from our key idea of learning a shared weight with deterministic random binary masks, whereas our sparse masks implicitly induce model capability.

Dropout. Dropout [23] is introduced as a training technique to avoid overfitting [27, 33], by randomly modifying neural network parameters or activations [45, 3, 49, 25, 17]. Although Dropout has been extended to compress neural networks [34, 35, 19], the *stochastic* dropping idea in Dropout can only be applied to standard and explicit neural architectures, which differs from the deterministic masks of our weight-tied models.

B Toolbox: CKA

Centered Kernel Alignment, proposed by [37], is a representation similarity measurement. It is invariant towards linear transformation, orthogonal transformation as well as isotropic scaling. We briefly outline the formulation of linear CKA below, where the CKA empowers the robust quantitation by normalizing the Hilbert-Schmidt Independence Criterion (HSIC) metric:

$$\text{CKA}(\mathbf{K}, \mathbf{L}) = \frac{\text{HSIC}(\mathbf{K}, \mathbf{L})}{\sqrt{\text{HSIC}(\mathbf{K}, \mathbf{K})\text{HSIC}(\mathbf{L}, \mathbf{L})}}. \quad (5)$$

Note that $\mathbf{X} \in \mathbb{R}^{m \times p_1}$ and $\mathbf{Y} \in \mathbb{R}^{m \times p_2}$ contain representations of two layers, with p_1 and p_2 neurons respectively. Each element of the $m \times m$ Gram matrices $\mathbf{K} := \mathbf{X}\mathbf{X}^\top \in \mathbb{R}^{m \times m}$ and $\mathbf{L} := \mathbf{Y}\mathbf{Y}^\top \in \mathbb{R}^{m \times m}$ represents the similarities between a pair of examples according to the representations in \mathbf{X} or \mathbf{Y} .

HSIC measures the similarity of centered similarity matrices and thus is invariant to orthogonal transformations of the representations as well as to permutation of neurons, namely $\text{HSIC}(\mathbf{K}, \mathbf{L}) := \frac{1}{(m-1)^2} \text{vec}(\mathbf{H}\mathbf{K}\mathbf{H})\text{vec}(\mathbf{H}\mathbf{L}\mathbf{H})$, where $\mathbf{H} = \mathbf{I} - \frac{1}{n}\mathbf{1}\mathbf{1}^\top$ is a centering matrix. More details can be found in [37].

C Experiment Details

For our baseline experiments, we use the open-source implementations provided by the respective authors. For MDEQ [5], we follow the settings provided in its open-source code and train the model using Adam optimizer with the cosine learning rate scheduler. The maximum learning rate is set to 0.001 with a weight decay of $2.5\text{e}-6$. The batch size is 64. For DEQ with *phantom gradient*, we follow the setting provided in [18] and use SGD with the cosine learning rate scheduler. The maximum learning rate is set to 0.2 with a weight decay of 0.0001. The batch size is set to 64. For both the MDEQ and DEQ with *phantom gradient*, the total epoch number is set to 50, 50, and 220 for Single-stream, Tiny and Large DEQ respectively. When comparing weight-tied models and DEQ models in Figure 2 and Table 1a, the training parameters of the weight-tied models are fixed to be of the same values as their corresponding DEQ models.

When training the multi-mask weight-tied models, we use different settings for the CIFAR-10 and ImageNet32 datasets.

- For ResNet models in CIFAR-10, we use Adam optimizer with a cosine learning rate scheduler. The maximum learning rate is 0.001 with a weight decay of $2.5\text{e}-6$. The model is trained for 150 epochs and batch size is 128.
- For CCT models in CIFAR-10, the AdamW optimizer is used with a cosine learning rate scheduler. The maximum learning rate is $6\text{e}-4$ and the model is trained for a total of 300 epochs, following CCT open-source code default settings.
- For Resnet models in ImageNet32, we use the SGD optimizer with a multi-step learning rate scheduler. The maximum learning rate is 0.05 with a weight decay of $1\text{e}-4$. The total epoch number is 90 and the batch size is 128.
- For CCT models in ImageNet32, we again use AdamW with a cosine learning rate scheduler. The maximum learning rate is $5\text{e}-4$ with a total training epoch of 300 instead.

During experimentation with the CIFAR-10 dataset, augmentations in the form of basic normalization, random cropping, and horizontal flipping are applied. We additionally perform experiments with ImageNet32. It consists of 32x32 images down-sampled from the original 224x224 images of ImageNet. ImageNet32 contains whole 1.2 million labeled training images and 150k test images distributed over 1,000 classes. All experiments are run on NVIDIA RTX 3090 GPUs.

D Additional Results

D.1 On the Ineffectiveness of DEQ

Computational inefficiency. Despite the elegance of the DEQ concept, the gradient estimation of these implicit models bottlenecks their practicality, due to the deficiency in both training and inference efficiency caused by the expensive Jacobian-inverse term or iterative Jacobian-vector products. For example, the Broyden solver used in DEQ [4] for exact gradient estimation would usually introduce over 30 iterations in the backward pass, leading to a prohibitive cost and causing severe slow-down when compared with standard explicit models. Though the implicit gradient estimation method (a.k.a. phantom gradient) proposed in [18] fastens [4] by at most $1.7\times$, it does not fully mitigate the efficiency issue due to the noticeable efficiency gap in Figure 2 (even after $1.7\times$ acceleration).

Optimization instability. In addition to the computational inefficiency, the training process of DEQs also exhibits instability [1]. Many DEQ variants, such as the original DEQ [4, 5] or DEQ with Jacobian regularization [6], indeed require employing a pre-training step by reusing DEQ layers in a weight-tied manner (stated in subsection 3.2), before entering the formal DEQ training with root-finding solvers. Such transition normally results in a remarkable performance drop, e.g. an approximated 5% drop can be observed in the 8-th epoch of Figure 10 (in Appendix D) when switching from the pre-training to DEQ training. The idea of Jacobian regularization [6] or phantom gradient [18] may alleviate this drop, but the gap, when compared to weight-tied ones, remains present as shown in Figure 10.

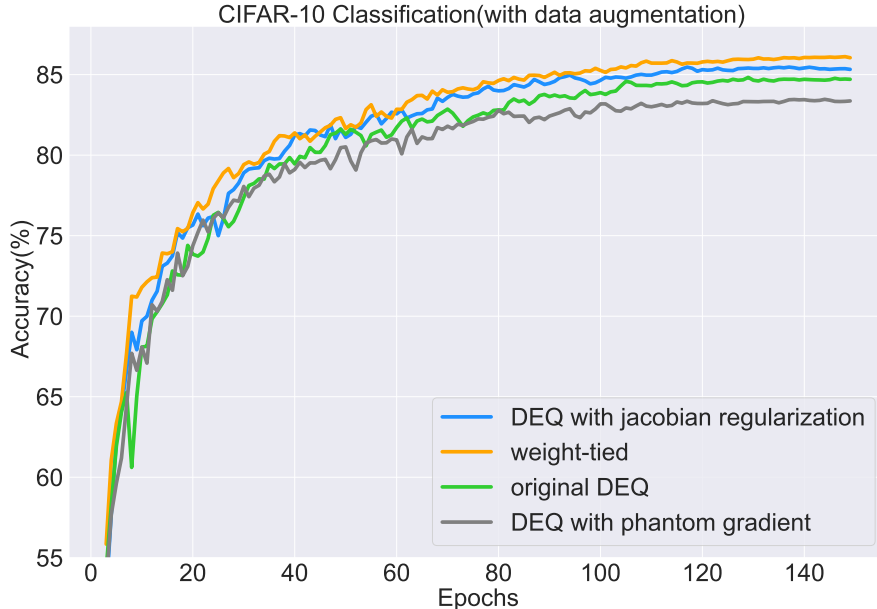


Figure 10: **The ineffectiveness and instability of DEQ variants over weight-tied models on the training dynamics.** The test is conducted using the ResNet model for CIFAR-10 image classification (w/ data augmentation). We depict the test accuracy over 150 training epochs, where the performance of various DEQ variants consistently under-perform the simple weight-tied model. All DEQ variants exhibit instability during training while the weight-tied model training is more stable. For fair comparison, we use Adam optimizer for all methods and use the hyper-parameters as suggested in the open-source implementations of each method. SGD optimizer is used in [18] for the phantom gradient; however, no dramatic difference can be observed in our evaluation.

D.2 Interpreting Multi-Mask Weight-Tied Model

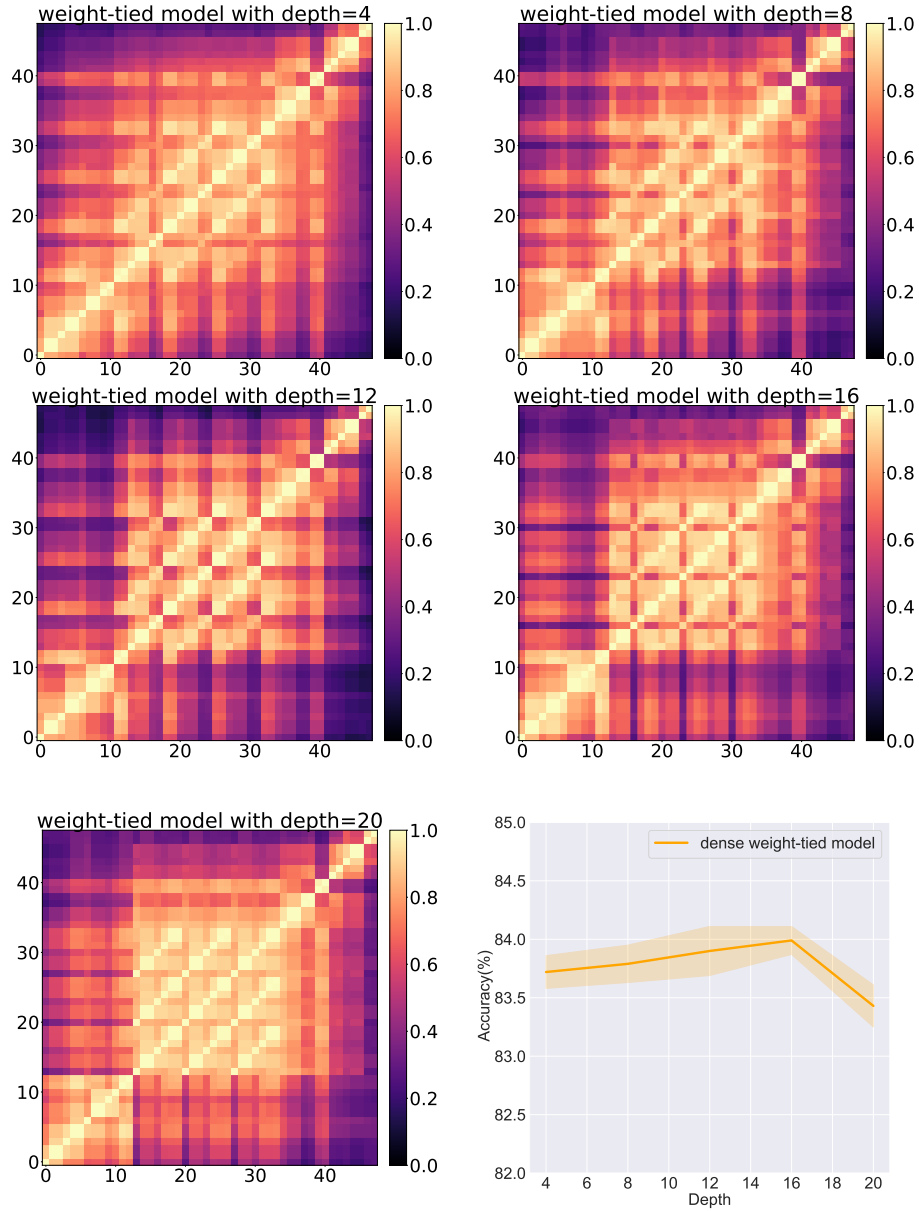


Figure 11: **Larger depth strengthens high output similarity pattern.** The figure shows layer output similarity and performance of dense weight-tied model under varying depths of 4, 8, 12, 16 and 20. The square color in position (i,j) represents the output similarity between the i -th layer and the j -th layer. To demonstrate this pattern more clearly, we have selected 4 tied-layers from each model, spaced evenly.